International Journal of Thin Films Science and Technology

http://dx.doi.org/10.18576/ijtfst/090202

Investigations In Structural Morphological And Optical Properties Of $Cd_{1-X}sn_xs$ Thin Films

M. N. Amroun[1,*], *A. H. Kacha* [2], *K. Salim* [1] *and M. Khadraoui* [1]

1 Laboratoire d'Elaboration et de Caractérisation des Matériaux, département d'électronique, Université Djilali Liabes, BP89, Sidi Bel Abbés 22000. Algeria
2 Laboratoire de Micro-électronique Appliquée, Université Djillali Liabès de Sidi Bel Abbès, 22000 Sidi Bel Abbès, Algeria.

Received: 2 Jan. 2020, Revised: 10 Feb. 2020, Accepted: 19 Feb. 2020

Published online: 1 May 2020

Abstract: $Cd_{1\_x}Sn_xS$ thin films with different concentrations x (x= 0 at%, 2 at%, 4 at%, 6 at% and 8 at %) were grown onto the glass substrates using spray pyrolysis technique. The structural, morphological and optical properties of pure CdS (x=0) and $Cd_{1\_x}Sn_xS$ ternary alloy thin films for different concentrations x were investigated. X-ray diffraction study showed that the deposited films were polycrystalline with hexagonal structure and the crystallinity of the CdS films has improved with Sn incorporation. The morphological and compositional properties of the deposited films have been investigated using scanning electron microscopy (SEM) and energy dispersive spectroscopy (EDS). SEM images revealed that tin addition caused notable changes in the surface morphology of the $Cd_{1\_x}Sn_xS$ thin films.
Also, the addition of Sn^{+2} ions improved the optical transmittance of the films. However, the optical absorption studies revealed that Sn addition did not change the absorption band gap of the prepared thin films. The variations of photocurrent density Jph of the pure CdS and $Cd_{1\_x}Sn_xS$ ternary alloy thin films have been investigated depending on Tin contents.
Keywords: CdS, $Cd_{1\_x}Sn_xS$, thin films, Optical properties.

1 Introduction

Recently, cadmium sulfide (CdS) has become an important compound semiconductor of II-VI group. CdS thin films have attracted the attention of many researchers due to their optical and electro-optical properties which serve in electronics and optoelectronic device applications, such as: transistors [1], photosensor [2], solar cell [3], gas sensor [4], light-emitting diodes (LEDs) in flat panel displays [5], etc. CdS exhibits the n-type conductivity with a band gap ~2.42 eV at room temperature. Depending on deposition conditions, CdS could be grown in two different structural phases: hexagonal (wurtzite) and/or cubic (zinc blende) [6].
The CdS thin films can be obtained using different methods, such as chemical bath deposition (CBD) [7], sputtering [8], electro deposition [9], vacuum evaporation [10] and spray pyrolysis [11, 12, 16]. Doping with Transition-metal (TM) elements, such as Cu [13, 14], In [15], Mn [17], Co [18], B [19], Fe [20] and Sn [21, 22] improves properties of CdS film.

The structural, morphological, optical and electrical properties of CdS thin films are strongly modified by the doping of TM elements (Sn^{+2}, Co^{2+}, Fe^{2+}…)[12,20,23] because of the sp–d exchange interaction between the localized d electrons of the transition metal magnetic ions and the mobile carriers in the conduction or valance band. The Sn^{2+} ion is an important transition metal element. The ion radius of Sn^{2+} (0.93Å) is smaller than that of Cd^{2+}(0.97 Å) ion indicating that Sn^{2+} can easily penetrate into CdS crystal lattice or substitute Cd^{2+} position in crystal [18]. $Cd_{1\_x}Sn_xS$ ternary alloy compounds are promising materials for many optoelectronic devices and solar cells applications [21.24]. $Cd_{1\_x}Sn_xS$ materials are both conductive and optically transparent in the visible region. Optical transparency in the visible region depends on the band gap of the alloy.
In the current contribution, we describe the fabrication of pure CdS films and Cd_{1_x} Sn_x S ternary alloy compound using spray pyrolysis technique and investigate their structural, morphological and optical properties by

*Corresponding author E-mail: amroun_mn@yahoo.com

comparing the same properties obtained in pure CdS and Cd_{1_x} Sn_x S ternary alloy thin films. So far, few pieces of literature have addressed the physical properties of $Cd_{1\_x}Sn_xS$ semiconductor thin films. To the best of our knowledge. The optical properties, such as the expected absorption capacity and photocurrent of the CdS and $Cd_{1\_x}Sn_xS$ ternary alloy thin films have not been reported in the literature yet.

2 Experimental Details

Pure CdS and $Cd_{1\_x}Sn_xS$ thin films with different concentrations x= 2 at%, 4 at%, 6 at% and 8 at%, films were deposited onto the glass substrates using spray pyrolysis technique at 300°C. The solution of pure CdS was prepared by dissolving a mixture of 0.1 M of the cadmium chloride ($CdCl_2$-$2H_2O$) and 0.1 M of thiourea (CH_4N_2S) in bi-distilled water [12]. Tin was added in $Cd_{1\_x}Sn_xS$ solution using $SnCl_2$ with several concentrations x (2 at%, 4 at% 6 at% and 8 at %) as the dopant source.The precursor solution of tin chloride ($SnCl_2.2H_2O$) was prepared using the solvent containing a mixture of deionized water and methanol in proper ratio. A few drops of HCl were also added for complete dissolutions to the solubility of $SnCl_2$.
The substrates were first cleaned in a water bath, followed by dipping in con. HCl, acetone and ethanol successively. Finally, the substrates were rinsed in deionized water and left to dry in a hot air oven. The distance between the nozzle and the substrates was kept at 29 cm with incident angle of 90°. Incomplete sentence. While the deposition rate was set to 8 ml/min, compressed air at a pressure (2 bar) has been used as a gas carrier. Moreover, the prepared solutions were immediately sprayed to avoid any possible chemical changes with time.
X-ray diffraction (XRD) patterns of the deposited films were recorded by Philips 1830 system using Cu Kα radiation (λ= 1.546 Å) with 2θ in the range 20 – 70°. The surface morphology and elemental analysis of the films were observed by a SEM (Joel JSM 5800 scanning electron microscope) and Energy-dispersive X-ray spectroscopy (EDS) under the operating voltage of 20 kV. The optical measurements were carried out at room temperature in the wavelength range 200 – 1500 nm using an UV (Ultra-Violet) Visible JASCO type V-570 double beam spectrophotometer.

3 Results and Discussion

3.1 Structural and Morphological Properties:

The structural properties of the pure CdS and Cd_{1-x} Sn_x S films have been investigated by XRD patterns. The XRD patterns of pure CdS and Cd_{1-x} Sn_x S thin films for different concentrations x (x=2 at%,4 at%, 6 at% and 8 at%) are presented in **Fig.1**. The reflection peaks were very narrowing and the existence of multiple diffraction peaks indicates the polycrystalline nature of the samples. All the observed peaks (1 0 0), (0 0 2), (1 0 1), (1 0 2), (1 1 0), (1 0 3), (1 1 2) (2 0 1), (2 0 2) and (2 0 3) planes are attributed to hexagonal wurtzite structure according to JCPDS card N° 41-1049 with a strong preferred orientation along (1 0 1) plane direction. T. Ozer et al. and Mehmet Peker et al. [21, 24] also reported the similar diffraction peaks for both pure CdS and Cd_{1-x} Sn_xS ternary alloy thin films deposited by spray pyrolysis technique at 300°C. No further reflection peaks in X-ray diffraction spectra were observed indicating the good structural quality of the prepared thin films. Moreover, the intensity of dominant peaks (101) increased by Sn incorporation, as shown in the inset of **Fig.2**, that revealed an improvement in the degree of polycrystallinity of the $Cd_{1-x}Sn_xS$ ternary alloy compound which leads to enhancement in the efficiency of the solar cells [25].

The structure of the deposited films can be observed through lattice constants calculation according to the Bragg formula $2\, d_{hkl} \sin\theta_{hkl} = n\lambda$. The lattice constants a and c of the hexagonal structure were estimated by the following expression [30]

$$\frac{1}{d_{hkl}^2} = \frac{4}{3}\left(\frac{h^2+hk+k^2}{a^2}\right) + \frac{l^2}{c^2} \qquad (1)$$

Where d is interplanar spacing and (hkl) are the miller indices. The obtained values of the lattice parameters 'a' and 'c' of the deposited films are listed in **Table.1.**
Table.1 indicates that the lattice constants values of the deposited films are consistent with the standard values taken from the JCPDS card previously cited. The lattice constants a and c of the pure CdS films are 4.1339 Å and 6.7124 Å, respectively. That is slightly lower than the standard results ($\Delta a \approx 0.0061$ Å, $\Delta c \approx 0.0066$ Å) which might be ascribed to effect of vacancies, defects and stress of CdS films. It also exhibits that the lattice parameters of the $Cd_{1-x}Sn_xS$ films changed with Sn concentration. These results imply that the Sn^{2+} has been incorporated into the crystal lattice of CdS films. The Sn^{2+} ions can easily enter into the crystal lattice of CdS and occupy the substitution or/and interstitially sites, knowing that the ionic radius of Sn^{2+} (0.93 Å) is smaller than that of Cd^{2+} (0.97 Å) [18].

The crystallite size (D), micro-strain (ε) and dislocation density (δ) were calculated using the relations [12, 27].

$$D = (0.9.\lambda)/(\beta.cos\theta) \qquad (2)$$

$$\varepsilon = \frac{\beta\cos\theta}{4} \qquad (3)$$

$$\delta = \frac{1}{D^2} \qquad (4)$$

The optoelectronic properties of the deposited thin films are affected by stacking fault probability (α*) due to the distorted lattice are estimated using the formula [26, 29]:

$$\alpha^* = \left(\frac{2\pi^2}{45(3tan\theta)^{1/2}}\right)\beta \qquad (5)$$

Where **λ** is the wavelength of Cu-Ka radiation, θ is the Bragg angle and β is defined as the full width at half maximum (FWHM) of the most intense diffraction peak (101). All the calculated crystalline parameters of the samples are summarized in **Table 1**.

Fig 3 shows the variation of average crystallite size, full width at half maximum (FWHM), Stacking fault (α*) and micro-strain (ε) values of the pure CdS (x=0) and $Cd_{1-x}Sn_x$ S ternary alloy compound for different concentration x (x=2 at%, 4 at%, 6 at% and 8 at %). It indicates that (FWHM) and the structural defects (the micro-strain (ε), dislocation density (δ), and Stacking fault (α*)) values decreased with Sn addition. This implies an increases in the average crystallite size (D) of the films from 20.34 nm for x=0 (pure CdS) to 24.32 nm for (x=8) indicating an improvement in the crystallinity of the Cd_{1-x} Sn_x S ternary alloy thin films. A similar results were reported by F.J. Willars-Rodríguez et al. **[**22**].** The crystallinity of the deposited films exhibit clear dependence on Sn concentration.

The texture coefficient for (101) orientation was estimated based on the following relation **[**28**].**

$$TC_{(101)} = \frac{I_{(101)}/I^0_{(101)}}{(1/N)\ \Sigma_n\, I_{(hkl)}/I^0_{(hkl)}} \qquad (6)$$

Where I (hkl) is the measured relative intensity of a plane (hkl). I° (hkl) is the standard intensity of the plane (hkl) taken from the JCPDS data, N is the reflection number and 'N' is the number of diffraction peaks. The calculated texture coefficients TC are listed in **Table 1**.

A sample with randomly oriented crystallite yields TC (h k l) = 1, while the larger this value, the larger abundance of crystallites oriented at the (h k l) direction.

Fig. 4 shows the variation of texture coefficient and crystallite size (D) of the Cd_{1-x} Sn_xS films with different Sn concentrations. A proportional relationship of the variation in the crystallite size and texture coefficients (Tc) was observed. The texture coefficient values of all the films are greater than one (>1) for the predominant (1 0 1) plane. The TC values had increased with Sn content, which may be attributed to the improvement in the crystallinity of the samples. These results indicate that the structural properties of CdS films are affected by tin content. The change of the nucleation and growth behaviour of CdS films upon Sn incorporation will further influence physical properties of the films. The obtained values of crystallite size and texture coefficient are consistent with those found by Waqar Mahmood et al **[**37**].**

Fig 5 illustrates the SEM micrographs of pure CdS and $Cd_{1-x}Sn_xS$ thin films prepared by the spray pyrolysis method at 300°C.

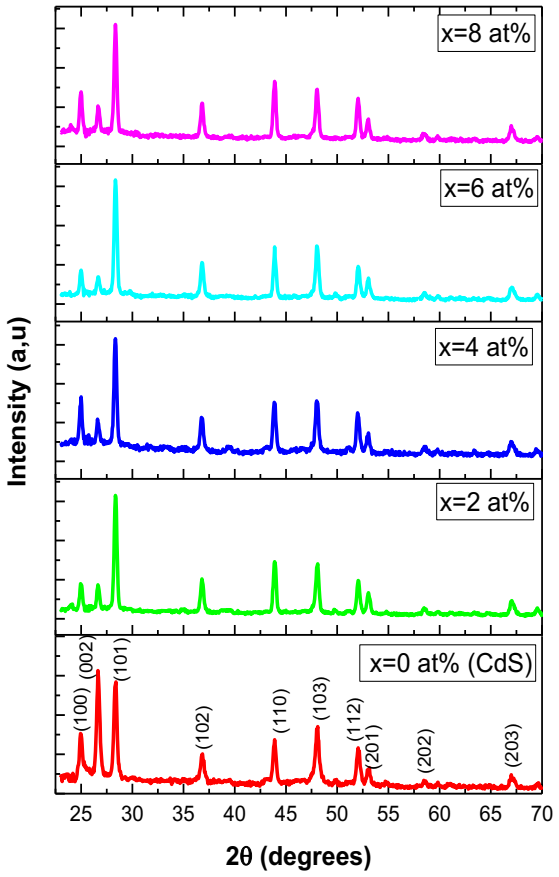

Fig.1: XRD pattern of pure CdS and Cd_{1-x} Sn_x S thin films for different concentrations x (x=2 at%, 4 at%, 6 at% and 8 at %) grown by spray pyrolysis technique at 300°C.

The micrographs indicated that the prepared films are dense and homogeneous surfaces. Nano-crystallized and no cracks are observed on large scan area. These images showed that the surface morphologies of the films were strongly dependent on the tin concentration. In addition, it is apparent that the increase of surface roughness after Sn incorporation results from the increase in the average crystallite size of the Cd_{1-x} Sn_x S films, which is also an evident from XRD.

The composition properties of the of pure CdS and Cd_{1-x} Sn_x S thin films have been defined by EDS spectra. The EDS spectra of the deposited thin films show the atomic ratio of Cd, Sn and S as also shown in **Fig.6** (A and B). It is obvious that Cd, Sn and S elements in the starting solutions are present in films. The presence of Si (the most intense peak) peaks may be due to the substrate effect.

Table.1: calculated the structural parameters of sprayed CdS and $Cd_{1-x}Sn_xS$ films with different x concentrations.

Concentration x (at %)	Lattice constants (Å)		FWHM (1 0 1) Peak (2θ°)	Crystallite size (D) (nm)	Dislocation Density(δ) (10^{-3}line/nm^2)	Strain (ε) (10^{-3})	TC (1 0 1) texture coefficient	Stacking fault (α*) (10^{-2} J /m^2)
	a	c						
CdS x=0 at%	4.1339	6.7124	0.4342	20.34	2.41	1.89	2.22	21.85
x = 2 at%	4.1275	6.7092	0.3814	23.156	1.86	1.66	3.07	19.19
x = 4 at%	4.1353	6.7238	0.3837	23.017	1.88	1.67	2.75	19.31
x = 6 at%	4.1332	6.713	0.3732	23.665	1.78	1.62	3.18	18.78
x = 8 at%	4.1352	6.710	0.36	24.32	1.69	1.56	3.10	18.12

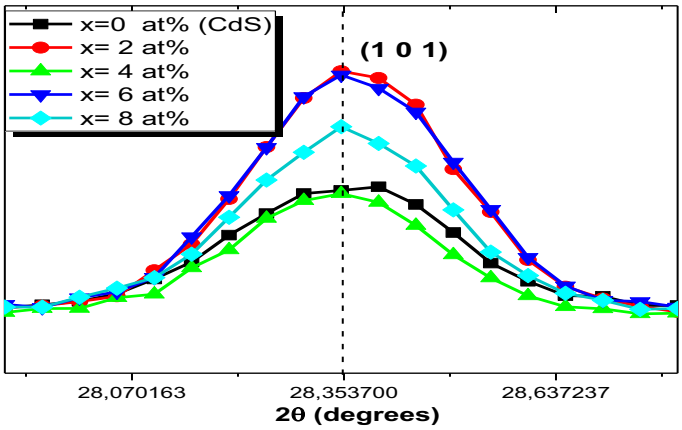

Fig. 2: (101) peak position of the pure CdS (x=0) and $Cd_{1-x}Sn_xS$ films for different concentrations x.

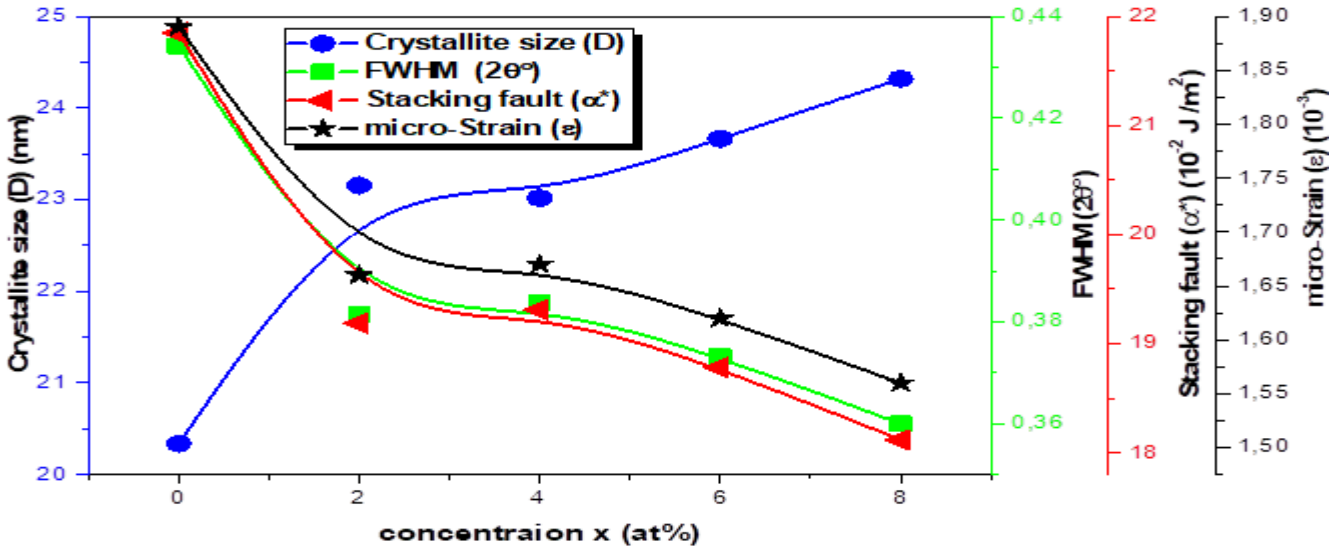

Fig. 3: the variation of average crystallite size, full width at half maximum (FWHM), Stacking fault (α*) and micro-strain (ε) of the pure CdS (x=0) and $Cd_{1-x}Sn_xS$ films for different concentration x (x=2 at%, 4 at%, 6 at% and 8 at %).

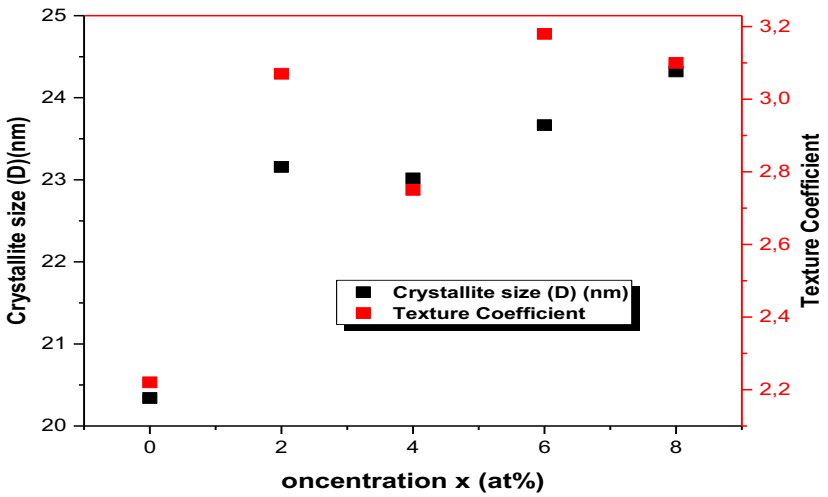

Fig. 4: Texture coefficient (TC) and crystallite size (D) of the samples as a function of tin concentration.

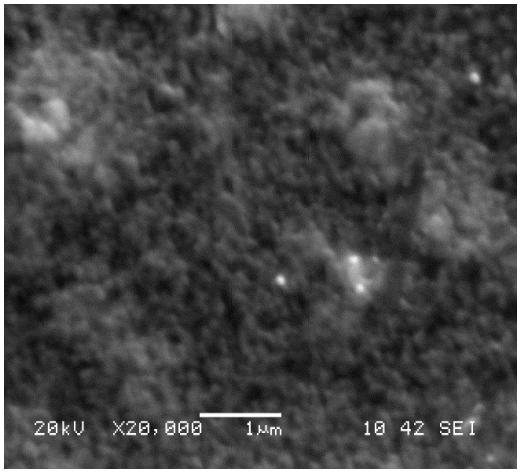

(a) x=0 at% (pure CdS)

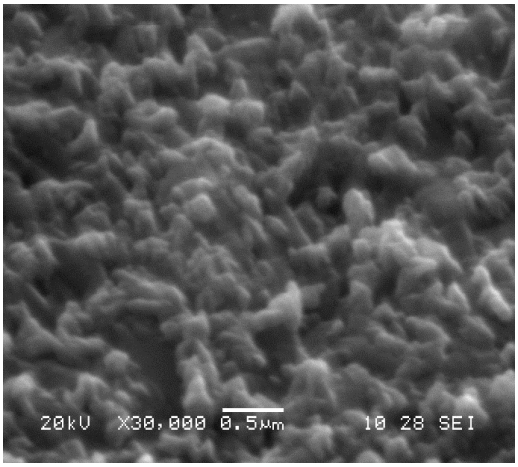

(b) x= 2 at%

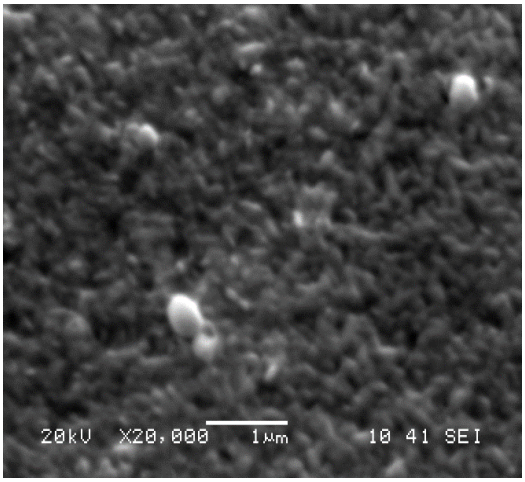

(c) x= 4 at%

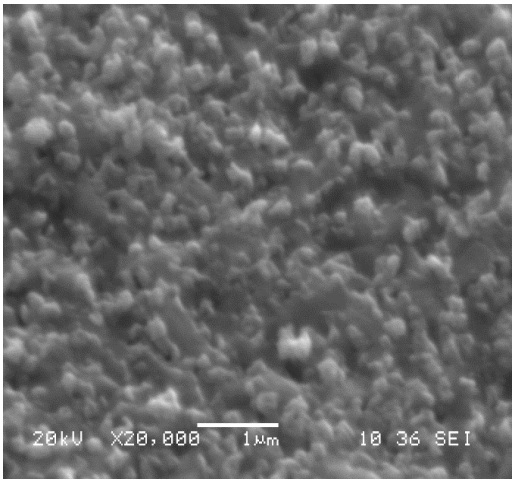

(d) x= 6 at%

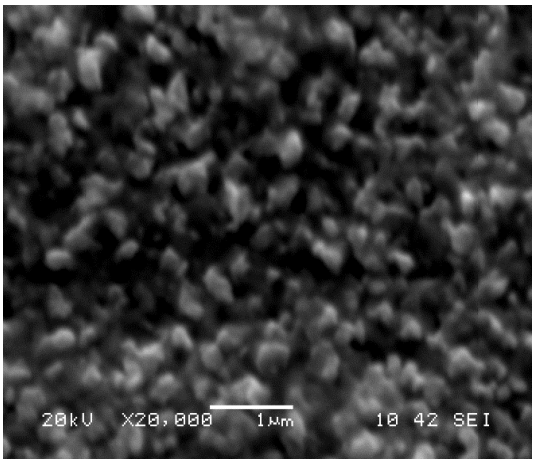

(e) x= 8 at%

Fig. 5: SEM micrographs of the Cd1-x Snx S films with different concentrations x (x=0 at%,2 at%, 4 at%, 6 at% and 8 at %).

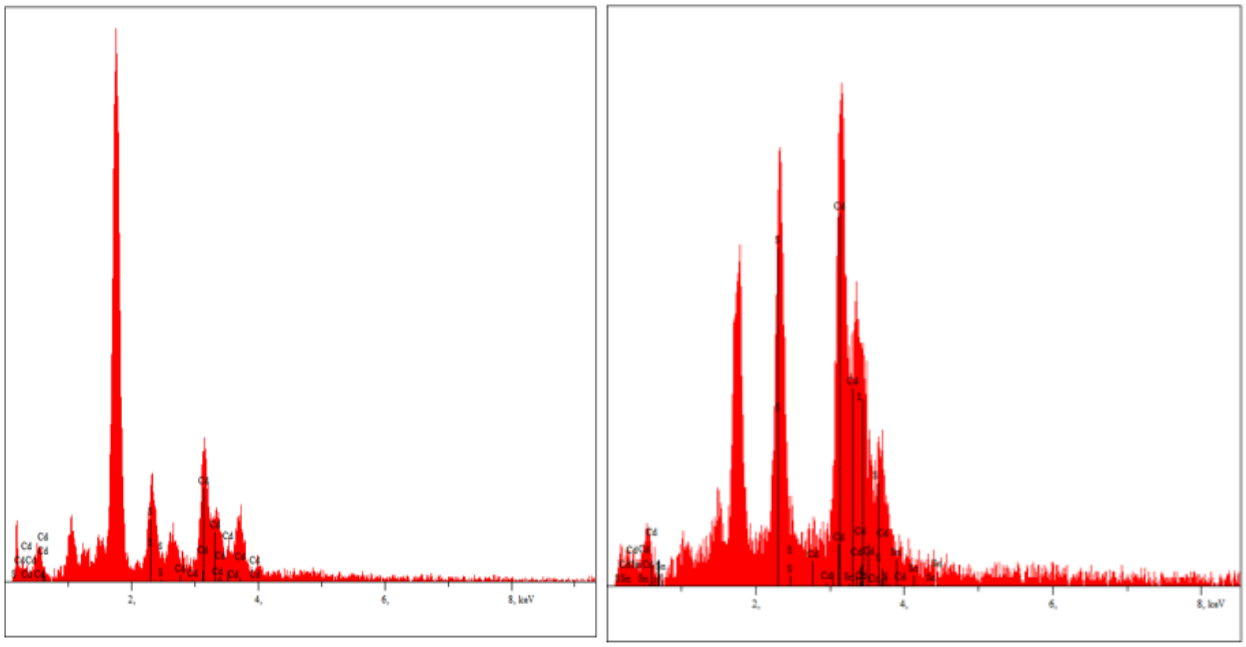

Fig. 6: EDS image of (A) pure CdS thin films to the left and (B) of Cd_{1-x} Sn_x S (x=8 at %) to the right Thin films.

3.2 Optical Properties

The transmittance substantially depends on surface roughness, oxygen deficiency and impurity levels. **Fig. 7 (A and B)** shows the optical transmittance (T) and reflectance (R) curves of the pure CdS and $Cd_{1-x}Sn_xS$ thin films grown with different concentration x as a function of incident light wavelength in 200 - 1500 nm.

The transmittance spectra of all the films (**Fig.7.A)** exhibited a transmission ratio, with a mean value around 70% in the visible and infrared region, and a sharp absorption edge around 500nm. The films exhibit a reflectance at a normal incidence less than 30% (**Fig.7.B).** The optical transmittance and reflectance spectra of $Cd_{1-x}Sn_xS$ films represent a strong dependence on the tin Content. It addition, the average transmittance of the films

increased with Sn introduction from 67% for pure CdS (x=0) at % at 77% for x=4 at%, indicating that the films have a rough surface with large crystallite size, which is consistent with SEM results. Increase in transmittance of the films with Sn incorporation might be ascribed to a rough surface with large crystallite size of the $Cd_{1-x}Sn_xS$ thin films **[32]**, which is consistent with SEM results. The results are consistent with those reported in the literature by K. C. Wilsonet al. **[**31**].**

The absorption coefficient (α) of $Cd_{1-x}Sn_xS$ thin films can be estimated using the obtained measurements of transmission (T), reflection (R) and thickness (d) data according to the equation **[**26**]**

$$\alpha = \frac{1}{d}\ln\left(\frac{(1-R)^2}{T}\right) \quad (7)$$

The variation of absorption coefficient of the deposited films with wavelength is shown in **Fig 8(A).** The calculated absorption coefficient of the samples are in the order of 10^4 cm^{-1}.

The energy band gap (Eg) of pure CdS and $Cd_{1-x}Sn_xS$ thin films could be estimated by assuming a direct transition between the valence band (E_V) and the conduction band (E_C) using the following equation **[**33**]:**

$$(\alpha h\upsilon)^2 = An\,(h\upsilon - E_g) \quad (8)$$

Where An is a constant, hυ is the photon energy and Eg the band gap energy. The precise value of optical band gap (Eg) is deduced from the intercept of the linear portion of the plot $(\alpha h\upsilon)^2$ as a function of photo energy (hυ) with energy axis, as shown in **Fig. 8(B).** The optical band gap energy (Eg) of the films is defined by extrapolating the straight-line portion of the plot at α = 0. The optical band gap values of the pure CdS and $Cd_{1-x}Sn_xS$ thin films for different concentrations x are 2.37 (±0.01) eV indicating that Sn addition in CdS lattice did not cause any significant changes to the optical band gap of CdS films. Similar results were also observed by **[**12, 21, 34**]** for $Cd_{1-x}Sn_xS$ thin films prepared by spray pyrolysis technique.

The optical band gap energy (Eg) of the samples can be also estimated from the relations **[**40, 41, 51**]**

$$E = \left[\frac{h^2}{8\pi^2 \times m^*}\right] K^{*2} \quad (9)$$

$$K^* = \frac{2\pi}{\lambda_a} = \frac{2\pi \times E_a}{hc} \quad (10)$$

Where E is the incident photon energy (hυ), h is the Planck constant, c denotes the speed of light, K^* is the wave number, Ea is the absorption energy of the material, (m^*) is the effective mass of the carrier at the Fermi level, m_e is the electron of masse (9.11×10^{-31} Kg). **Fig 9** shows the graphical representation of the energy E as function of square of the wave number K^2 for pure CdS and $Cd_{1-x}Sn_xS$ thin films for different concentrations x. The extrapolation of the linear portion of the plot onto the energy axis (Fig 9) gives an optical band gap of the samples varied between 2.32 and 2.34 eV, which are comparable with the value obtained previously from the optical absorption measurements 2.37(±0.01) eV. The difference of band gap obtained from this optical measurements was only 0.02 eV. Such small value could be due to the measurement incertitude. The obtained values are consistent with those found by S. Kose et al **[**50**]** for Cu doped CdS films grown by ultrasonic spray pyrolysis technique. The incorporation of impurity into the semiconductor often reveals the formation of band tailing in the band gap in the exponential edge region. Urbach energy can be defined using the following expression **[**35**].**

$$\boldsymbol{\alpha = \alpha_0 \exp\,(h\upsilon/E_u)} \quad (11)$$

Where α_0 is a constant, hυ is the photon energy and E_u is the urbach energy, which represents the degree of disorder. It is also called the urbach energy which gives the width of the band tail of the localized state of the band gap **[**36**].**The urbach tail (Eu) is defined from the reciprocal of the slope of the linear portion of a plot of ln (α) against hv, as shown in inset Fig 10. The maximal urbach energy of 0.236 eV was obtained for pure CdS films. The urbach energy reduced with Sn addition, reaching a minimum of about 0.169 eV for x=4 at. Then, it slightly increased for x= 6 at% and x= 8at% at 0.19 eV and 0.22 eV, respectively. The decrease of urbach energy values of the CdS films with Sn incorporation can be attributed to the improvement of films quality. These results are consistent with XRD data. The obtained values of urbach energy are better than those reported in the literature **[**38, 39**].**

To investigate the effect of pure CdS and $Cd_{1-x}Sn_xS$ buffer layer on solar-cell performance, the expected absorption capacity and photocurrent of the pure CdS and $Cd_{1-x}Sn_xS$ ternary alloy thin films were defined using the measured absorption coefficient data. Assuming a thin films-based solar cell with perfect antireflection, no absorption in the upper layers and normal incidence. The thickness-dependent absorbed photon fraction and the photocurrent are calculated by the following relations [26, 42, 51]:

$$Absorbed\ photon\ fraction = \frac{\int_{300\,nm}^{\lambda g} F(\lambda)(1-\exp(-\alpha(\lambda)d))\,d\lambda}{\int_{300\,nm}^{\lambda g} F(\lambda)\,d\lambda} \quad (12)$$

$$J_{ph}(d) = q \times \int_{300\,nm}^{\lambda g} F(\lambda)(1-\exp(-\alpha(\lambda)d))\,d\lambda \quad (13)$$

Where: $\alpha(\lambda)$ is the wavelength-dependent optical absorption coefficient of the film, $F(\lambda)$ is the AM1.5G photon flux, q is the electron charge and the wavelength $\lambda_g = hc/E_g$. In **Fig 11** (A and B), we have reported the evolution of the absorbed photon fraction and the photocurrent of the pure CdS and Cd_{1-x} Sn_xS thin films for different concentrations x. One can observe that the Sn incorporation has a significant effect on the performance of the CdS thin films. The pure CdS films exhibit high absorption fraction and photocurrent of 36 mA/cm^2 for layer thickness greater than 2000 nm.

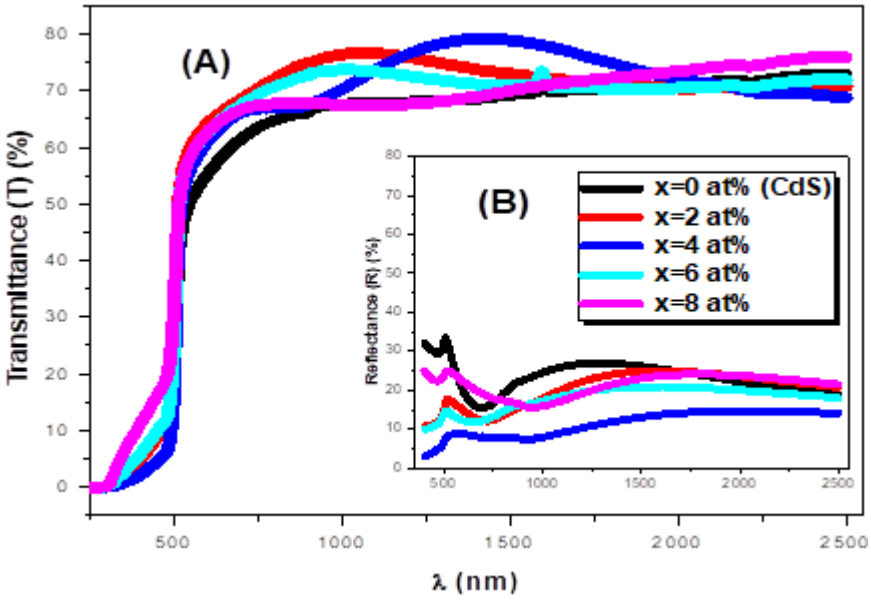

Fig.7: Transmission (A) and Reflection (B) spectrum of pure CdS and for $Cd_{1-x}Sn_xS$ thin films (x= 2, 4, 6, and 8 at %).

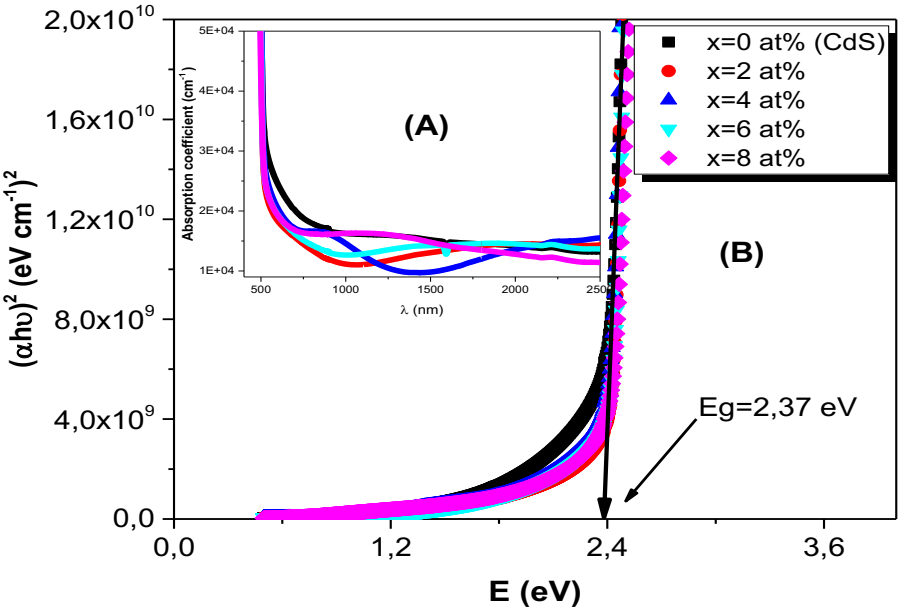

Fig.8: Variation of absorption coefficient (A), plot $(\alpha h\upsilon)^2$ versus (E) (B) of pure CdS and $Cd_{1-x}Sn_xS$ thin films for different concentrations x.

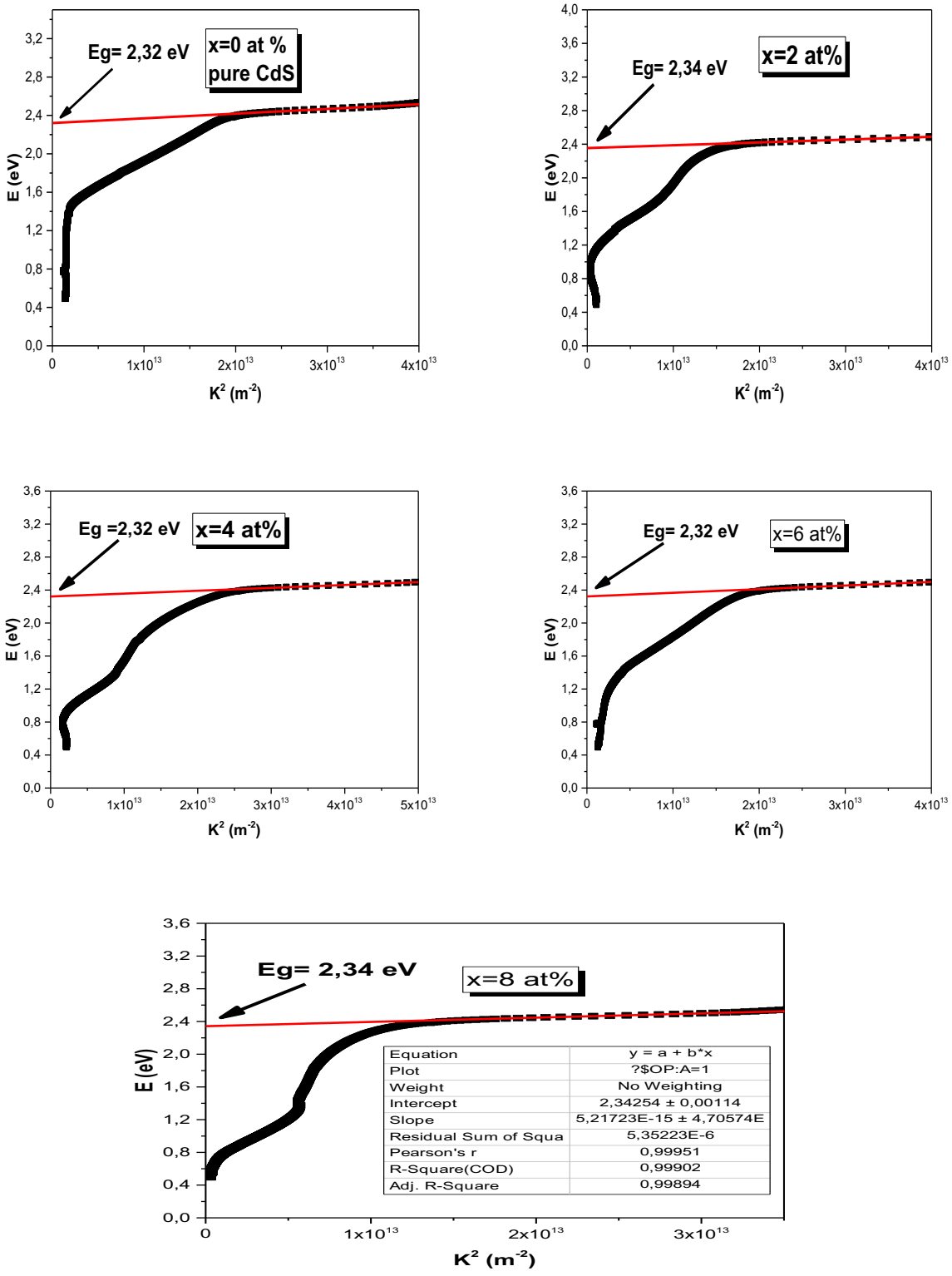

Fig 9: Photon energy E as a function of K^2 of pure CdS and $Cd_{1-x}Sn_xS$ thin films (x= 2, 4, 6, and 8 at %)

The refractive index (n) of semiconducting materials plays a very important role in optical communication and designing spectral dispersion, optical and optoelectronic devices. The refractive index depended on several factors, including the electronic polarizability, local fields of semiconducting material and transmission. Thus, it is important to define this parameter for the CdS films using the following relation **[**43**]:**

$$n = \frac{1+R}{1-R} + \sqrt{\frac{4R}{(1-R)^2} - k^2} \quad (14)$$

$$k = \frac{\alpha\lambda}{4\pi} \quad (15)$$

Where R is the reflectance at room temperature, λ denotes the wavelength of the incident photon and k the extinction coefficient. ε_1 and ε_2 are the real and imaginary part of the dielectric constant respectively. The variation of refractive index (n) with wavelength of the samples shown in **Fig. 12 (A).** The refractive index (n) of the films decreased from 3.75 to 1.9 with varying Sn concentration from x=0 (pure CdS) to x=4at% over the spectral range from 480 nm to 2500 nm. Decreases in the refractive index with Sn addition could be attributed to the reduction in the density of the film materials or the increase in the surface roughness $Cd_{1-x}Sn_xS$ alloy thin films. Due to its straightforward link with the dispersion energy, the refractive index (n) remains an important physical property of materials dedicated to optical devices. The reduction of the refractive index n of the CdS films with Sn addition was observed in literature **[**22**].**

The refractive index dispersion could be examined using Wemple-DiDomenico model of single oscillator, which describes the dielectric response for transitions below the inter-band absorption edge. In the region of low absorption the photon energy dependence of the refractive index dispersion, n is expressed by **[**47**].**

$$n^2(E) - 1 = \frac{E_0 E_d}{E_0^2 - E^2} \quad (16)$$

Where E_d is the dispersion energy (is a measure of the average strength of inter-band optical transitions) and E_0 is the average excitation energy for electronic transitions (single oscillator energy). The oscillator parameters were determined from the slope $(E_d.E_o)^{-1}$ and intercept E_o / E_d at the vertical axis of the variation of $(n^2 - 1)^{-1}$ as a function of E^2. The obtained values of (E_0, E_d) are illustrated in **Table 2.** The average strength of inter-band optical transitions E_d of the CdS thin films is strongly influenced by Sn incorporation. It ranges between 7.82 eV to 11.55 eV and increases with Sn addition. The maximum of E_0 (4.92 eV) occurs for x= 4 at%. The obtained values are comparable with those reported by **[**48**]** for CdS thin films prepared by electron beam vacuum evaporation technique.

The loss rate of the power of a mode of oscillation is measured using the dissipation factor. The dissipation factor (tanδ) of the deposited films is calculated using the relation **[**44, 45**]**

$$\tan\delta = \frac{\varepsilon_2}{\varepsilon_1} \quad (17)$$

Where ε_1 and ε_2 are the real and imaginary parts of the complex dielectric constant (ε) and are related to refractive index (n) and extinction coefficient (k) via the relationships **[**43**]**:

$$\varepsilon_1 = n^2 - k^2 \quad (18)$$

$$\varepsilon_2 = 2nk \quad (19)$$

Fig 12 (B) shows the variation of dissipation factor of all the thin films with the wavelength. The dissipation factor of all the films decreases sharply with increasing wavelength between 400 and 750 nm (visible region), and thereafter slightly increased at higher wavelength. This suggests that the interaction between photons and electrons takes place in the thin films at low wavelength region.

The real ε_1 parts of the dielectric constant can be expressed by the relation **[**49**]**

$$\varepsilon_1 = \varepsilon_\infty - \left[\left(\varepsilon_\infty * \omega_p^2\right)/\omega^2\right] \quad (20)$$

Where ε_∞ is the high frequency dielectric constant, ω_p is the plasma resonance frequency and ω is the angular frequency. The value of plasma frequency (ω_p) and high dielectric constant (ε_∞) deduced from the slope and intercept of the (ε_1) against (ω^{-2}) plot **Fig 12 (C).** The obtained values are reported in **Table 2.** The value of ε_∞ was defined from the intercept of the extrapolating straight line with ε_1 axis. From **Table 2,** we note a monotonic increment of the plasma frequency (ω_p) with the composition x is of the order of 10^{+14} s^{-1}.

Table 2: Optical parameters of sprayed CdS and $Cd_{1-x}Sn_xS$ films with different x concentrations.

Composition x	E_d (eV)	E_0 (eV)	ε_L	ε_∞	ω_p (s^{-1})
Pure CdS	7.82	3.72	5.79	5.96	$4.45 \times 10^{+14}$
x=2 at%	8.81	4.39	4.78	4.51	$8.61 \times 10^{+14}$
x=4 at%	9.99	4.92	3.06	3.37	$9.43 \times 10^{+14}$
x=6 at %	11.03	4.33	4.56	3.92	$6.14 \times 10^{+14}$
x=8 at%	11.55	3.70	5.68	6.86	$9.92 \times 10^{+14}$

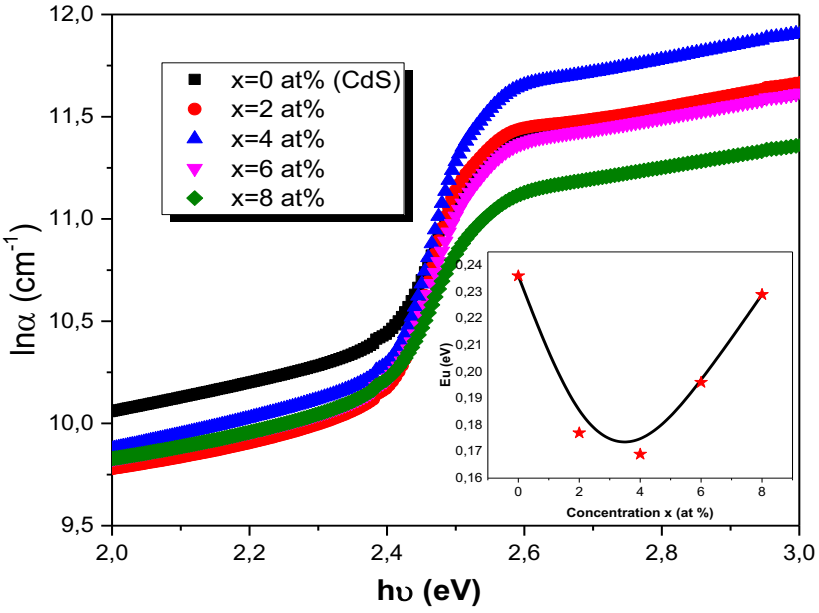

Fig. 10: plot ln (α) against (hυ) of pure CdS and $Cd_{1-x}Sn_xS$ thin films for different concentration x.

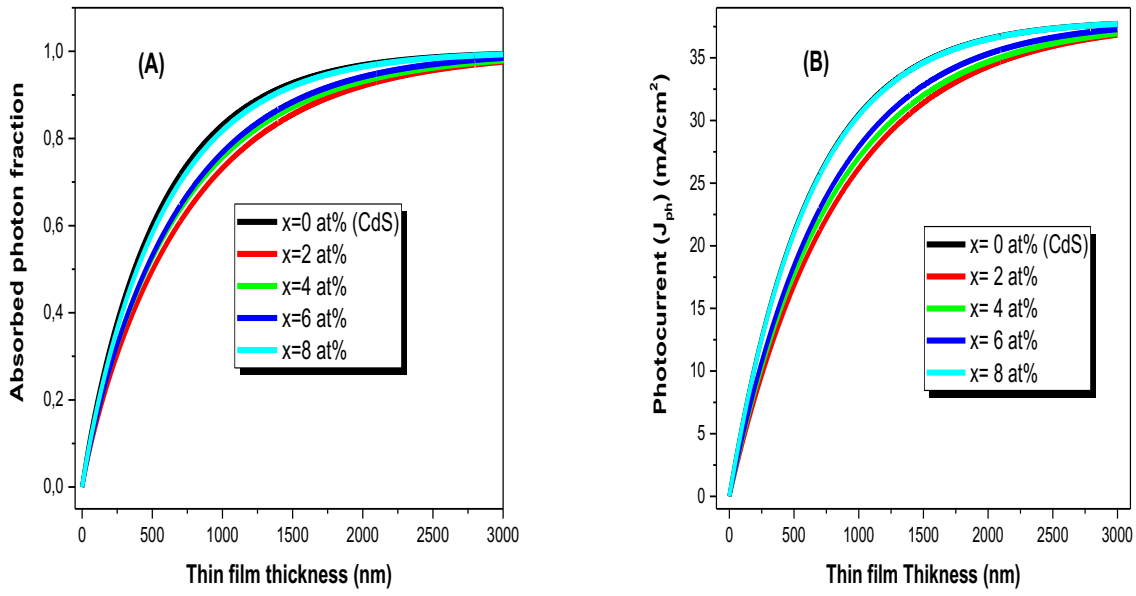

Fig. 11: (A) absorbed photon fraction, (B) photocurrent of pure CdS and $Cd_{1-x}Sn_xS$ thin films for different concentration x.

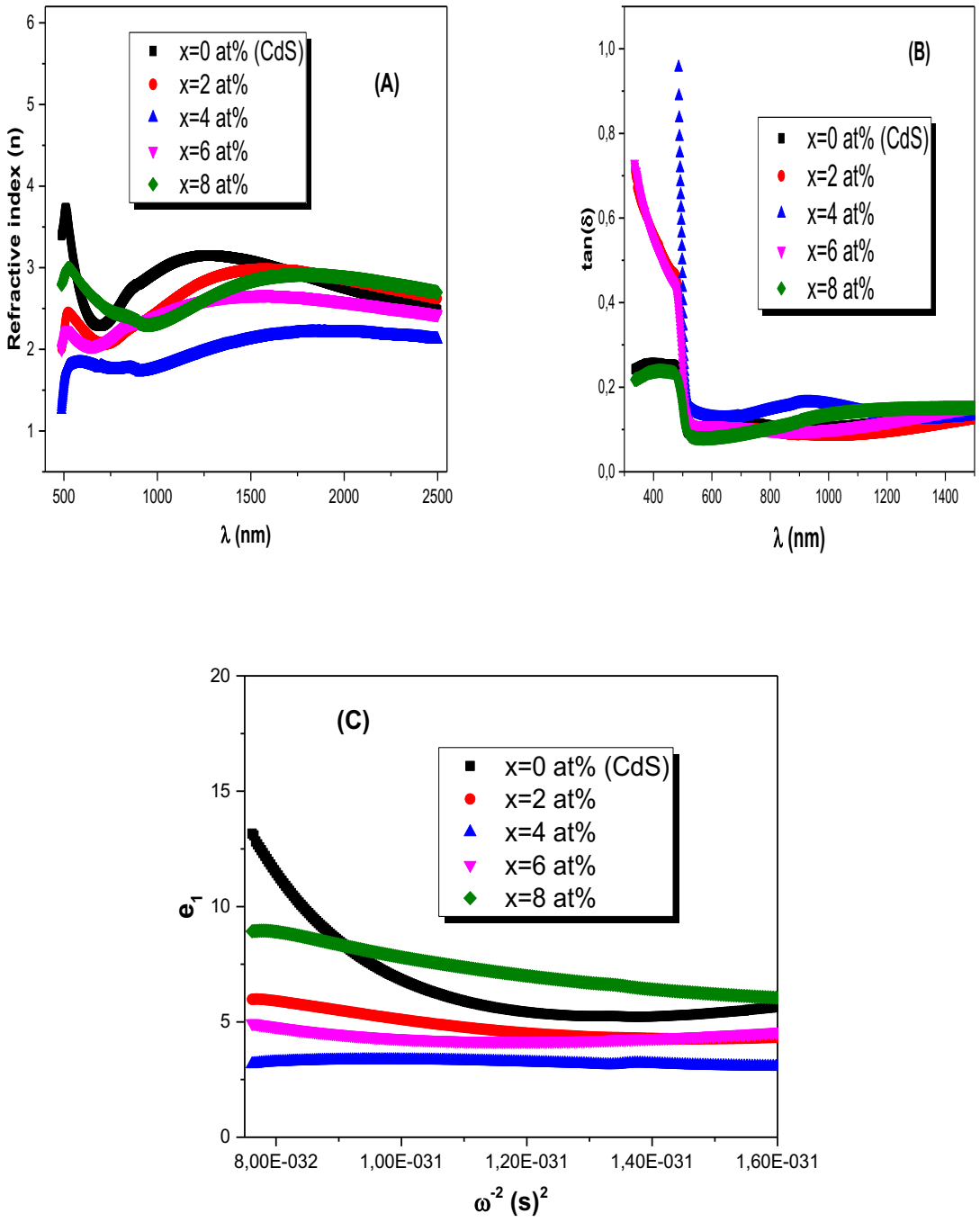

Fig 12: The variation of (A) the refractive index, (B) dissipation factor and (C) the real ε_1 parts of the dielectric constant of pure CdS and $Cd_{1-x}Sn_xS$ thin films for different concentration x.

4 Conclusion

Nanostructured pure CdS thin film and Cd_{1-x} Sn_xS ternary alloy thin films for different concentrations x= 2%, 4%, 6% and 8% were grown on glass substrates at 300°C using the spray pyrolysis technique. The XRD analysis shows that the films are polycrystalline with hexagonal phases and average crystallite size ranging from 20.34 to 24.32 nm. The structural defects, such as the stress, dislocation density and stacking fault of the CdS films decreased significantly with Sn addition. The optical band gap was defined from optical absorbance data with two different methods. Inaddition, the band gap of the CdS films did not significantly change with the Sn introduction. It was also seen that the effective mass of the carrier changed by the Sn content. The photocurrent density J_{ph} was 36 mA/cm^2 at thin film thickness above 2000 nm. In this study, the refractive index dispersion was analysed using the single oscillator model. The refractive index ranges between 3.75 to 1.9 over the visible and infrared region. The optical constants, such as the dissipation factor, high frequency dielectric constant and the plasma resonance frequency were also evaluated and strong dependency on Sn content was observed.

The present study showed that the Sn addition improves the physical properties of the CdS films which can be useful for optoelectronics and solar cells applications.

References

[1] W. Wondmagegn, I. Mejia, A. Salas-Villasenor, H. Stiegler, M. Quevedo-Lopez, R.Pieper, B. Gnade, Microelectron. Eng., **157**, 64-70(2016).

[2] B. G. An, Y. W. Chang, H. R. Kim, G. Lee, M. J. Kang, J. K. Park, J. C. Pyun, Sens.Actuators., **B 221**, 884-890(2015).

[3] I. P. Liu, L. Y. Chen, Y. L. Lee, J. Power Sources., **325** 706-713(2016).

[4] S. T. Navale, A. T. Mane, M. A. Chougule, N. M. Shinde, J. H. Kim, V. B. Patil, RSC Adv., **4,** 44547-44554(2014).

[5] T.T. Xuan, J.Q. Liu, R.J. Xie, H.L. Li, Z. Sun,Chem. Mater., **27**, 1187-1193(2015).

[6] A. Slonopas, H. Ryan, B. Foley, Z. Sun, K. Sun, T. Globus and P. Norris, Materials Science in Semiconductor Processing., **52**, 24-31(2016).

[7] A. I. Oliva, O. Solıs-Canto, R. Castro-Rodrıguez, P. Quintana, Thin Solid Films., **391**, 28-35(2001).

[8] M. A. Islam, M. S. Hossein. , M. M Aliyu, P. Chelvanathan, Q. Huda, M. R. Karim, K. Sopian, N. Amin. Energy Procidia.,**33**, 203-213(2013).

[9] V. R.P. Raffaelle, H. Forsell, T. Potdevin, R. Fridefeld, J. G. mantovani, S. G. Bailey, S. M. Hubbard, E. M. Gordon and A. F. Hepp, Sol. Energy Mater. Sol. Cells., **57,** 167(1999).

[10] K. Senthil, D. Mangalaraj, Sa. K. Narayandass, Applied Surface Science., **169-170**, 476-479(2001).

[11] Tariq Abdulhamid Abbas, Jala Muhamed Ahmad, Journal of Electron Devices.,**17**, 1413-1416(2013).

[12] M.N. Amroun, M. Khadraoui, R. Miloua, Z. Kebbab, K. Sahraoui. Optik., 131, 152–164(2017).

[13] D. Petre, I. Pintilie, E. Pentia, I. Pintilie, T. Botila, Mater. Sci. Eng., **B 58**, 238–243(1999).

[14] Y. Kashiwaba, K. Isojima, K. Ohta, Sol. Energy Mater. Sol. Cells., **75**, 253–259(2003).

[15] F. Atay, V. Bilgin, I. Akyuz, S. Kose, Mater. Sci. Semicond. Process., **6**, 197–203(2003).

[16] F. Taghizadeh Chari, M. R. Fadavieslam, Optical and Quantum Electronics https://doi.org/10.1007/s11082-019-2081-8., 51-77(2019).

[17] D. Sreekantha Reddy, K. Narasimha Rao, K.R. Gunasekhar, N. Koteeswara Reddy,K. Siva Kumar, P. Sreedhara Reddy, Mater. Res. Bull., **43** 3245–3251(2008).

[18] R. Sathyamoorthy, P. Sudhagar, A. Balerna, C. Balasubramanian, S. Bellucci, A.I. Popov, K. Asokan, J. Alloys Compd., **493**, 240–245(2010).

[19] J. Lee, Thin Solid Films 451–452 (2004) 170–174.

[20] B. Tripathi, F. Singh, D.K. Avasthi, A.K. Bhati, D. Das, Y.K. Vijay, J. Alloys Compd., **454**, 97–101(2008).

[21] T. Ozer, S. Kose, Int. J. Hydrogen Energy., **34,** 5186–5190(2009).

[22] F.J. Willars-Rodríguez, I.R. Chávez-Urbiola, M.A. Hernández-Landaverde, P.Vorobievc, R. Ramírez Bon and Yu. V. Vorobiev, thin solid films, **653,** 341-349(2018).

[23] S. Aksaya, M. Polat, T. Ozer, S. Kose, G. Gurbuz, Applied Surface Science., **257**, 10072– 10077(2011).

[24] Mehmet Peker , Derya Peker,M.Selami Kılıckaya. Physica., **B 405**, 4831–4837(2010).

[25] Subhash Chander, M.S. Dhaka, thin solid films., **638** 179-188(2017).

[26] M.N. Amroun, M. Khadraoui,Optik., **184**, 16-27(2019).

[27] R. Mariappan, V. Ponnuswamy, P. Suresh, R. Suresh, M. Ragavendar; Superlattices and Microstructures., **59** 47–59(2013).

[28] Chafia Khelifi, Abdallah Attaf, Hanane saidi, Anouar Yahia, Mohamed Dahnoun, Surfaces and Interfaces., **15,** 244–249(2019).

[29] N. Anitha, M. Anitha, L. Amalraj, Optik., **148**, 28–38(2017).

[30] M.N. Amroun, M. Khadraoui, R. Miloua, N. Benramdane, K. Sahraoui, Z. Kebbab, journal pf optoelectronique and advanced materials., **19**, 771 – 777(2017).

[31] K. C. Wilson, E. Manikandan, M. Basheer Ahamed, and B. W. Mwakikunga, J. Alloys Compd., **585**, 555(2014).

[32] M. Anitha, K. Saravanakumar, N. Anitha, I. Kulandaisamy, L. Amalraj, Materials Science & Engineering., **B 243** 54–64(2019).

[33] M. Khadraoui, R. Miloua, A. Benramdane, K. Bouzidi, Mater. Chem. Phys., 1–7(2015).

[34] J.C. Orlianges, C. Champeaux, P. Dutheil, A. Catherinot, T. Merle Mejean, Thin Solid Films., **519** 7611–7614(2011).

[35] F. Urbach, Phys. Rev., **92**, 1324(1953).

[36] J. Olley, Solid State Communications**13**, 1437-1440 (1973).

[37] Waqar Mahmood, Junaid Ali, Iqra Zahid, Andrew Thoma,Anwar ul Haq, Optik.,**158**, 1558–1566(2018).

[38] Ameen M. Ali, Yulisa Yusoff, Lamya M. Ali, Halina Misran, Md. Akhtaruzzaman,Mohammad A. Alghoul, Kamaruzzaman Sopian, Shahidan Radiman, Nowshad Amin, Solar Energy., **173**, 120–125(2018).

[39] T. Hurma, Optik., **127**, 10670–10675(2016).

[40] R.A. Serway, C.J. Moses, C.A. Moyer, Modern Physics, 2nd ed., Saunders College Publishing, New York., 188(1997).

[41] N. Koteeswara Reddy, K.T. Ramakrishna Reddy, Materials Research Bulletin., **41,** 414–422(2006).

[42] R. Khadraoui, N. Miloua, A. Benramdane, K. Bouzidi, Mater. Chem. Phys., 1–7(2015).

[43] A.Mary Saroja, I.Kartharinal Punithavathy, S.Johnson Jeyakuma, S.Joshua Gnanamuthu, A.R.Balu, Optik., 130,245-254 (2017).

[44] Z. Serbetci, R.K. Gupta, F. Yakuphanoglu, J. Sol-Gel Sci. Technol., **61**, 477–483(2012)

[45] A.M.M. Tanveerkarim, M.K.R. Khan, M. Mozibur Rahman,Mater. Sci. Semicond. Process., **41**, 184–192(2016).

[46] S.H. Wemple, M. DiDomenico, Phys. Rev., **B 3** 1338(1971).

[47] A.S. Hassanien, A.A. Akl, , J. Alloys Compd., **648** 280-290(2015).

[48] Subhash Chander, M.S. Dhaka, thin solid films., **638**, 179-188(2017).

[49] F.Z. Bedia, A. Bedia, N. Maloufi, M. Aillerie, F. Genty, B. Benyoucef, Journal of Alloys and Compounds., **616** 312–318(2014).

[50] S. Kose, F. Ataya, V. Bilgin, I. Akyuz, E. Ketenci, Applied Surface Science., **256** (2010) 4299–4303

[51] M.N. Amroun et al. Effect of TM (TM= Sn, Mn, Al) Doping on the Physical Properties of ZnO Thin Films Grown by Spray Pyrolysis Technique: A comparative Study. Int. J. Thin.Film. Sci. Tec. http://dx.doi.org/10.18576/ijtfst/., **9(1)**, (2020).